Electrochimica Acta 179 (2015) 482–494

Contents lists available at ScienceDirect

Electrochimica Acta

journal homepage: www.elsevier.com/locate/electacta

On the electrochemistry of tin oxide coated tin electrodes in lithium-ion batteries

Solveig Böhme*, Kristina Edström, Leif Nyholm[1]

Department of Chemistry - Ångström Laboratory, Uppsala University, Box 538, SE-751 21 Uppsala, Sweden

ARTICLE INFO

Article history:
Received 5 December 2014
Received in revised form 17 February 2015
Accepted 17 February 2015
Available online 19 February 2015

Keywords:
Tin oxide
Lithium-ion batteries
Electrochemistry
CV
XPS

ABSTRACT

As tin based electrodes are of significant interest in the development of improved lithium-ion batteries it is important to understand the associated electrochemical reactions. In this work it is shown that the electrochemical behavior of SnO_2 coated tin electrodes can be described based on the SnO_2 and SnO conversion reactions, the lithium tin alloy formation and the oxidation of tin generating SnF_2. The CV, XPS and SEM data, obtained for electrodeposited tin crystals on gold substrates, demonstrates that the capacity loss often observed for SnO_2 is caused by the reformed SnO_2 layer serving as a passivating layer protecting the remaining tin. Capacities corresponding up to about 80 % of the initial SnO_2 capacity could, however, be obtained by cycling to 3.5 V vs. Li^+/Li. It is also shown that the oxidation of the lithium tin alloy is hindered by the rate of the diffusion of lithium through a layer of tin with increasing thickness and that the irreversible oxidation of tin to SnF_2 at potentials larger than 2.8 V vs. Li^+/Li is due to the fact that SnF_2 is formed below the SnO_2 layer. This improved electrochemical understanding of the SnO_2/Sn system should be valuable in the development of tin based electrodes for lithium-ion batteries.

1. Introduction

Lithium-ion batteries are on their way of becoming the main system for rechargeable batteries since they can store more energy per unit volume and weight than nickel-metal hydride, lead-acid or nickel-cadmium batteries. In commercial lithium-ion batteries graphite is currently the most commonly used anode material. However, graphite has a limited volumetric and gravimetric capacity which is a drawback when higher energy densities are required, for instance, in cars or power plants. [1–4] Tin could therefore be an alternative anode material which could increase the capacity of a full cell by up to 10 %.

There are more than thousand articles describing different aspects of tin and tin-based compounds as anode materials in lithium-ion batteries. The reason for this large interest is the high energy density of tin (theoretical specific capacity: 991 $\frac{mAh}{g}$) and its potential to provide high power densities. Tin is also interesting because of the challenging chemistry occurring when lithium alloys with tin leading to a large volumetric change. Reactions with the electrolyte at the interface of tin particles has received a lot of scientific interest in attempts to improve the performance of tin and tin-based electrodes. Despite all these efforts there is still a lack of detailed fundamental studies regarding the electrochemical reactions taking place during charge and discharge [1–4].

However, it is not only metallic tin which is of importance but also tin(IV) oxide and tin(II) oxide. [2–6] Tin(IV) oxide and tin(II) oxide give theoretical specific capacities of about 1491 mAh/g and 1270 mAh/g, respectively, due to a combination of both the oxide conversion reaction and the alloying reaction involving the formed metallic tin. The alloying of tin gives a theoretical specific capacity of 991 mAh/g (see Reactions 1 and 2 below) which can be compared to that of 372 mAh/g for the intercalation reaction of graphite. As has been pointed out by many authors this clearly shows the advantage of using tin oxides as anode materials in lithium-ion batteries [6,3,7].

$$2xLi^+ + 2xe^- + SnO_x \rightarrow xLi_2O + Sn \quad (1)$$

$$4.4Li^+ + 4e^- + Sn \rightleftharpoons Li_{4.4}Sn \quad (2)$$

During the alloy formation on the first cycle there is also a formation of a Solid Electrolyte Interphase (SEI) as the organic solvents used in the electrolyte are not thermodynamically stable below about 0.8 V vs. Li^+/Li. [8–11] It has, however, recently been reported that the SEI could be formed even at potentials between 1.2 V and 1.5 V vs. Li^+/Li [12,13].

Earlier reports have on the other hand proposed that the electrochemical reaction taking place at 1.2 V vs. Li^+/Li involves an irreversible conversion of tin oxide to tin and lithium oxide as

* Corresponding author. Tel.: +0046 18 471 7321.
E-mail address: solveig.bohme@kemi.uu.se (S. Böhme).
[1] ISE member.

http://dx.doi.org/10.1016/j.electacta.2015.02.150
0013-4686/

described in Reaction 1. (The standard potentials of SnO_2 and SnO 1.566 V and 1.585 V, respectively.) [14,6,15] As a result of the conversion reaction, a lithium oxide matrix is thus formed which encloses the tin particles. At potentials below 0.9 V vs. Li^+/Li the alloying reaction described in Reaction 2 (which results in a large volume change) can subsequently be observed [3–6,14–21].

Chouvin et al. [17,18] have shown that the conversion of SnO to tin is reversible to some extent when cycling above 0.3 V vs. Li^+/Li. With the help of X-ray absorption, ^{119}Sn-Mössbauer spectroscopy and X-ray diffraction the reformation of SnO upon charge could thus be demonstrated. The authors explained this based on the assumption that the $Sn-O$ interactions in the Sn/Li_2O matrix get weaker when a lot of lithium is alloyed with tin and that the tin agglomerates at lower potentials. The latter was assumed to render the reoxidation of tin to SnO more difficult [17,18].

Both the SEI formation and the conversion reaction are consequently generally assumed to be irreversible reactions occurring only on the first cycle. This gives rise to a large capacity loss which is the main problem associated with the use of tin oxides as anode materials in lithium-ion batteries. Little information can, however, be found about the electrochemical behavior of the native tin oxide layer which always forms on tin in contact with air or water. Nevertheless, there are many reports on the use of nanosized SnO_2-structures, some of which displayed a certain degree of reversibility for the conversion reaction in lithium-ion batteries. The latter has generally been attributed to the presence of nanoparticles or the use of additives such as copper or carbon [6,14,15,17–19,22].

The focus of this study is mainly to study the electrochemical reactions of tin oxides above 0.9 V vs. Li^+/Li, i.e., between 0.9 V and 3.0 V vs. Li^+/Li in detail. It is within this potential range that there is a controversy regarding which electrochemical reactions that occur and the explanations for the reversibility of tin oxide reactions that has been found. Traditionally, there has been a large focus on the volume changes during the alloying reaction of tin at lower potentials since this leads to cracking and pulverization of the material and thus the loss of electrical contact upon extended cycling. [4–6,17,18,23–25] There are hence many reports describing different methods to circumvent the volume expansion [2–4,26,27], but only relatively few reports deal with the electrochemical reactions taking place at higher potentials.

To study the different electrochemical reactions in detail it is important to avoid the influence of binders and carbon black (electronic additives) normally used in composite electrodes for lithium-ion batteries. In the present work electrodeposition was therefore used for the manufacturing of tin oxide coated tin crystals on gold substrates.

Electrodeposition is a method which offers several advantages compared to other conventional synthesis routes. Electrode materials can be directly deposited on a metallic substrate which later can serve as a current collector. In addition, the depositions are carried out at low temperatures and the approach is also suitable for large scale production. [28,29] There are many reports in the literature about the electrodeposition of tin mainly involving depositions from tin(II) solutions containing complexing agents like tartrates or citrates to avoid whisker formation [30–34].

In the present work, tin films were formed on gold substrates via electrodeposition from a tin(IV) ion solution containing citrate as the complexing agent. In this way the use of binders and other additives that could give rise to additional electrochemical reactions during the cycling in the lithium-ion batteries was avoided. The reason for using gold as the substrate was that most metals which commonly are used as substrates, e.g., copper or nickel form alloys with tin. As these alloys also are able to incorporate lithium they interfere with the electrochemical reactions due to tin and tin oxide. Although gold also forms alloys with lithium [35–37], this reaction only takes place below about 0.2 V vs. Li^+/Li which means that these electrochemical reactions readily can be separated from those involving the lithium-tin alloy.

A native nanometer thick layer of tin oxide was formed subsequent to the electrodepostion and some samples were also oxidized further electrochemically to study the electrochemical behavior of tin oxide in more detail. The electrochemical behavior of these tin/tin oxide coatings as anode materials in lithium-ion batteries was studied in order to gain information about the electrochemical processes taking place mainly during cycling at high potentials. To facilitate the interpretation of the results, XPS was also employed to study the surface composition of the electrodes subjected to different potentials.

2. Experimental

2.1. Electrodeposition

The solution used for the electrodeposition contained 0.2 M tin(II) chloride hydrate (Sigma Aldrich, > 98 %) and 0.4 M trisodium citrate dihydrate (Sigma Aldrich, > 99 %). The pH of the solution was adjusted to 4 with concentrated hydrochloric acid (VWR, 37 %).

Prior to the depositions tin(II) was oxidized to tin(IV) by blowing air through the deposition solution for three hours at 85 °C based on the work by Chang et al. [38].

20 ml of the oxidized solution were then placed in an electrochemical cell containing a gold disc (Goodfellow, 99.95 %; 15 mm diameter, 0.1 mm thickness) working electrode which thus served as the substrate during the tin deposition. The gold discs had previously been cleaned with ethanol (Solveco, 99,5 %) for 10 minutes in an ultrasonic bath at room temperature. The employed counter electrode was a platinum wire and the reference electrode was an $Ag/AgCl$ electrode containing saturated KCl. The electrodeposition was carried out chronopotentiometrically with a cathodic current density of 5 mA/cm^2 for 120 s and 300 s, respectively, in order to obtain different film thicknesses. The tin films were subsequently washed with deionized water.

To produce thicker tin oxide layers than the native oxide layers formed in contact with air some films were oxidized electrochemically immediately after the electrodeposition. The oxidation was carried out in the form of recording linear scan voltammograms from 0 V to +0.8 and +1 V vs. $Ag/AgCl$, respectively, at a scan rate of 10 mV/s. The anodization was thus carried out in the same cell and the same electrolyte as used in the electrodeposition step.

2.2. Characterization of the tin films

X-ray diffraction patterns were recorded with a Siemens D5000 Diffractometer with a T2T fixed x-ray tube using a parallel plate collimator (Soller) 0.40 and the software Diffrac plus XRD commander 2.4 from Bruker.

The XPS spectra recorded prior to the electrochemical experiments were obtained with an ESCA Quantum 2000 from Physical Electronics (PHI) using a monochromatic Al K_α X-ray source. An analyzer pass energy of 23.5 eV was employed while the corresponding value was 58.7 eV for the recording of the XPS profiles. Calibration of the binding energy scale was carried out based on the hydrocarbon surface contamination C 1s peak at 285.0 eV and the peaks were analyzed using a non-linear Shirley-type background. The software Casa XPS was used to fit curves to the obtained spectra.

The SEM micrographs were obtained employing a SEM LEO 1550 from Zeiss.

2.3. Electrochemical behavior in lithium-ion batteries

Prior to cell assembly the tin oxide coated tin electrodes were dried for 12 hours at 120 °C in a vacuum furnace (Büchi Glass oven

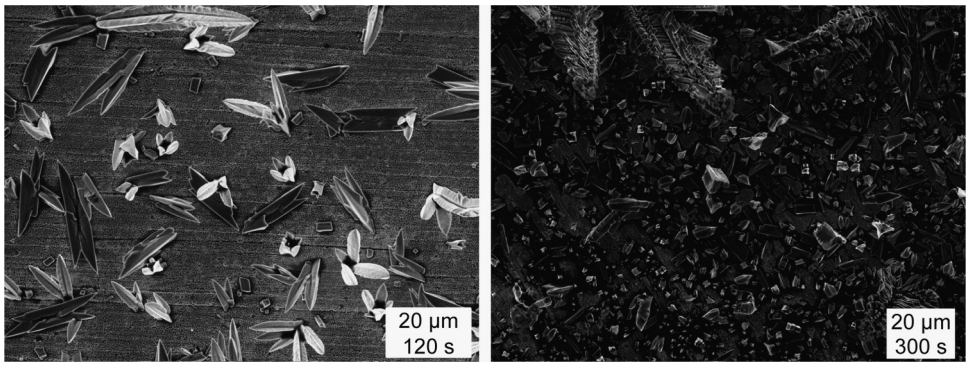

Fig. 1. SEM images of the tin crystals on deposited the gold surface for a deposition time of 120 s and 300 s, respectively.

B-585). The electrochemical behavior of the electrodes was then studied in a two-electrode pouch cell containing a lithium foil as the counter electrode and a glass fiber as separator employing cyclic voltammetry. Three drops of 1 M $LiPF_6$ dissolved in a mixture of 1:1 ethylene carbonate and diethyl carbonate was used as the electrolyte.

The cyclic voltammograms (CVs) were recorded with a BioLogic SA VMP2 instrument using the EC-Lab software and a scan rate of 1 mV/s. Each CV was recorded with a new sample.

2.4. Characterization of cycling products

XPS was employed to study the results of the electrochemical reactions above 2.5 V vs. Li^+/Li. The spectra were recorded for samples cycled to 2.5 and 3.5 V vs. Li^+/Li, respectively. The batteries were dismantled in an argon-filled glove box and the electrodes were rinsed with DMC (dimethylcarbonate) prior to transfer to the XPS chamber using a special built transfer system to avoid contact with air. The XPS spectra were measured with a PHI 5500 Multi-Technique system (Perkin Elmer) using a monochromatic Al K_α X-ray source and a pass energy of 23.5 V. The pressure in the analysis chamber was about $3 \cdot 10^{-9}$ bar. Calibration of the binding energy scale was carried out based on the hydrocarbon surface contamination C 1s peak at 285.0 eV and the peaks were analyzed using a non-linear Shirley-type background. Fingerprint spectra were recorded at the beginning and at the end to ensure that no damage to the samples due to the x-ray radiation had occurred during the measurements. The software Casa XPS was used to fit curves to the obtained spectra.

SEM micrographs of the cycled electrodes were taken using a SEM LEO 1550 from Zeiss.

3. Results and Discussion

3.1. Electrodeposition Reactions

As described in the experimental section, the electrodepositions were carried out using a tin(IV) solution containing citrate. The tin complex most likely to form in solutions containing tin(IV) ions (Sn^{4+}) and citrate anions ($Hcit^{3-}$) is [$Sn(cit)$] which should result in a liberation of one proton from the citrate. The latter is due to the fact that upon formation of the tin(IV) complex [$Sn(cit)$], the citrate hydroxyl group is deprotonated as well as this complex is more stable than in which the tin binds solely to the carboxyl groups [39].

The deposition reaction, which involves a release of citrate anions cit^{4-} is described in Reaction 3.

$$[Sn(cit)] + 4e^- \rightarrow Sn + cit^{4-} \quad (3)$$

The liberated cit^{4-} anions then react with water to form hydroxide ions and the more stable $(Hcit)^{3-}$ anion, according to Reaction 4 [40].

$$cit^{4-} + H_2O \rightarrow (Hcit)^{3-} + OH^- \quad (4)$$

A chronopotentiogram for the electrodepostion employing a constant cathodic current of 5 mA/cm^2 for 300 s is shown in the supporting information. During the electrodeposition the potential dropped to about −0.88 V during the first 100 s and then increased to a stable potential of −0.85 V. These potentials are clearly much more negative than the standard potentials for the reduction of tin(IV) and tin(II) ions (i.e., 0.13 V and −0.14 V, respectively) as a result of the shift in the reduction potential due to the formation of the citrate complex.

After the electrodeposition the tin surface reacted with oxygen in air or water to form a native tin oxide layer of several nanometers as is shown in Reaction 5 [41,42].

$$Sn + \frac{x}{2}O_2 \rightarrow SnO_x \quad (5)$$

Thicker tin oxide layers were obtained by an electrochemical oxidation employing linear sweep voltammetry (carried out in the deposition electrolyte) based on Reaction 6.

$$Sn + xH_2O \rightarrow SnO_x + 2H^+ + 2e^- \quad (6)$$

3.2. Characterization of the tin films (composition and thickness)

During the electrodeposition, tin crystals were deposited on the gold substrate and these tin crystals were subsequently coated with a native tin oxide layer. As is seen in Fig. 1a deposition time of 120 s gave rise to a relatively low tin surface coverage while a significantly higher surface coverage was found after deposition for 300 s. A closer look at the SEM image in Fig. 1b, however, shows that a full surface coverage was not reached even after 300 s which means that the electrode should be regarded as tin oxide coated tin crystals present on a partially visible gold substrate. Films deposited for 300 s were used in all the characterizations and electrochemical experiments described below, unless stated otherwise.

To investigate the chemical composition of the films XRD and XPS were mainly used. A Raman spectrum and its interpretation can, however, also be found in the supporting information. The XRD patterns are presented in Fig. 2, mainly show reflections due to gold and tin, although reflections due to a tin gold alloy also can be observed after the deposition for 120 s (Fig. 2).

These latter reflections were, however, not visible for the film deposited for 300 s most likely due to the presence of a thicker tin layer.

The presence of tin oxide at the surface of the tin crystals could be proved with Raman spectroscopy (see the supporting information) and XPS. As is shown in Fig. 3, a native tin oxide layer could

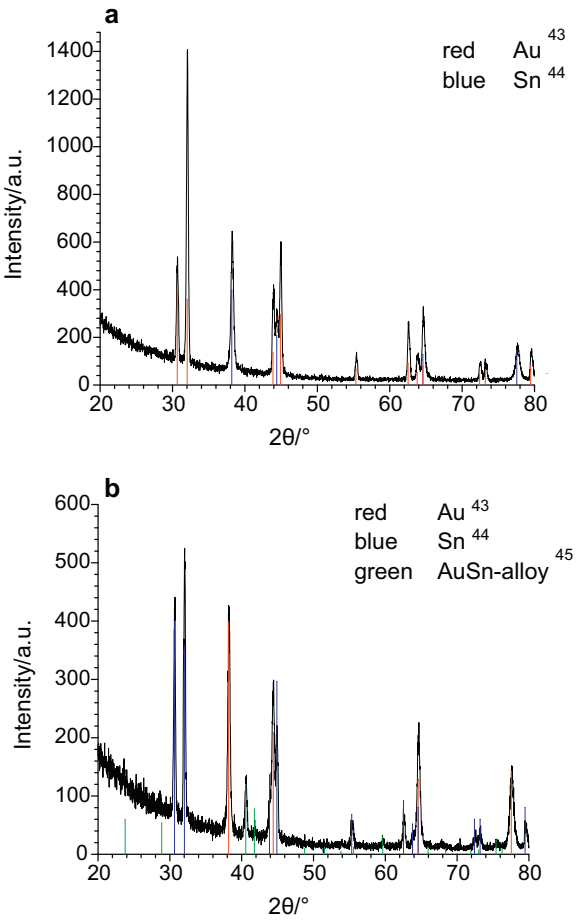

Fig. 2. XRD patterns for the tin films deposited on the gold surface using a deposition time of a) 300 s and b) 120 s. The reference data were taken from references 43, 44 and 45 [43–45].

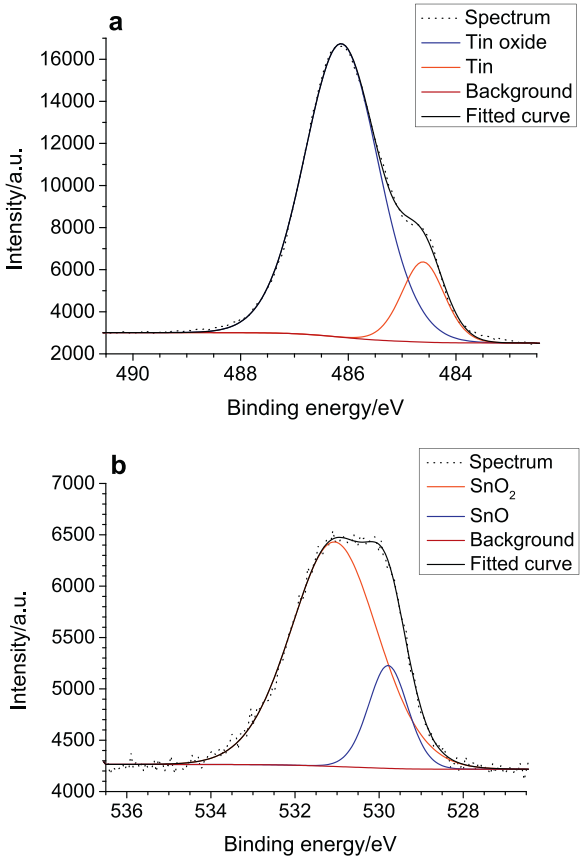

Fig. 3. XPS spectra with curves fitted to a) the Sn $3d\frac{5}{2}$ peak and b) the O 1s peak.

hence be detected on the surface of the tin crystals. In the XPS spectra, which include the fitted curves and peaks two signals were thus present in the Sn $3d\frac{5}{2}$ spectrum. The signal at the lower binding energy (red curve; 484.61 eV; 13.57 %) indicates the presence of elemental tin while the broader peak at the higher binding energy (blue curve; 486.13 eV; 86.43 %) indicates the presence of tin oxide [46].

As is seen in Fig. 3, two curves could be fitted to the O 1s spectrum. The latter were assigned to SnO_2 (red curve; 531.06 eV; 82.8 %) and *SnO* (blue curve; 529.79 eV; 17.2 %), respectively. It is reasonable to assume that the SnO_2 was present on top of the SnO layer and that the native tin oxide layer thus contained both Sn(IV) and Sn(II) oxide.

Fig. 4 shows XPS depth profiles for the tin coatings obtained with a deposition time of 300 s. From the depth profiles, which were made by Ar^+ etching, it is seen that the oxygen intensity dropped to zero after about 60 s of etching and that the tin intensity simultaneously reached its maximum. Although, it is difficult to calculate the thickness of the tin oxide layer based on the etching results, a sputter time of 60 s translated into a layer thickness of about 6 nm according to the software. The latter value should be compared with the thickness of about 3.5 nm which previously has been reported for native tin oxide layers. [41,42] It should, however, be pointed out that the native oxide layer depends on the experimental conditions and that thicker layers generally are found for samples immersed in aqueous electrolytes. It is therefore reasonable to assume that the tin oxide layers were thicker than 3.5 nm particularly as the electrodepositions were carried out in aqueous solutions. [41,42] A thickness of about 6 nm as obtained from the etching results therefore seems as a reasonable value for the native tin oxide film. This is also in good agreement with the Raman spectrum results (see the supporting information) which indicate the presence of a nanometer thick tin oxide layer (see the supporting information).

XPS spectra were also recorded for the samples oxidized using linear voltammetric scans to +0.8 V and +1 V vs. *Ag*/*AgCl*, respectively (see Fig. 4). For the samples anodized to +0.8 V vs. *Ag*/*AgCl*, a sputter time of 120 s was required to reach an oxygen signal intensity of zero which translated into a tin oxide layer thickness of 12 nm. For the sample anodized to +1 V vs. *Ag*/*AgCl* a sputter time of 240 s was analogously required which corresponded to a tin oxide layer thickness of 24 nm.

Even though, the absolute tin oxide layer thicknesses remain unknown, the sputter results indicate that the relative sputter times can be used to estimate the relative thicknesses of the tin oxide layers. It is thus reasonable to assume that tin oxide layer on the sample anodized to +0.8 V vs. *Ag*/*AgCl* was about twice as thick as the native tin oxide layer. Analogously, the tin oxide layer on the sample anodized to +1 V vs. *Ag*/*AgCl* should have been approximately four times the thickness of the native tin oxide.

In Fig. 4 it is also seen that the oxygen intensity did not decrease in a linear manner with increasing sputter depth, at least, for the anodized samples. One reason for this could be that SnO_2 was present on the surface of the layer while mainly *SnO* was present deeper down in the oxide layer in good agreement with the XPS spectrum in Fig. 3.

Based on the characterization of the tin oxide coated tin crystals with respect to thickness and composition it hence is clear that the sizes of the tin crystals were of the order of several micrometers large (see Fig. 1) while the thickness of the tin oxide layers were of the order of nanometers. It is likewise clear that the tin based

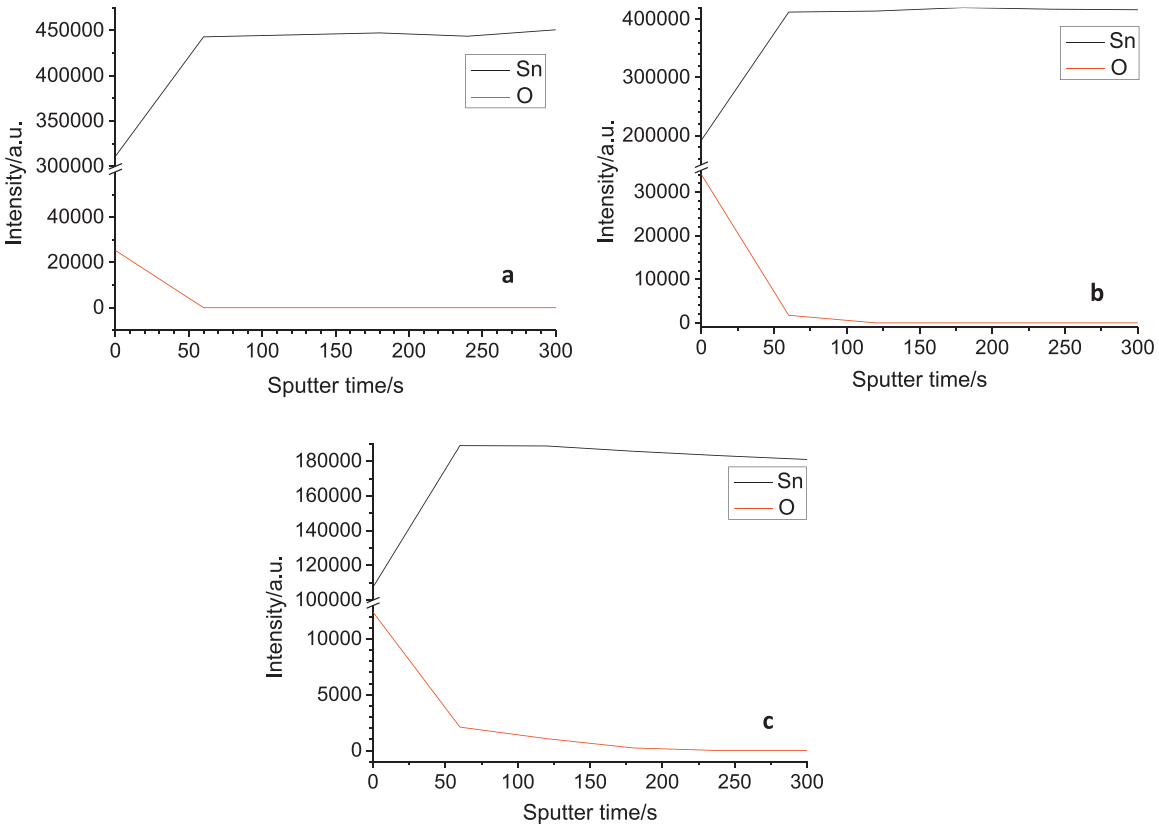

Fig. 4. XPS tin and oxygen depth profiles for a) the native tin oxide layer b) the sample anodized at +0.8 V vs. *Ag*/*AgCl* and c) the sample anodized at +1 V vs. *Ag*/*AgCl*.

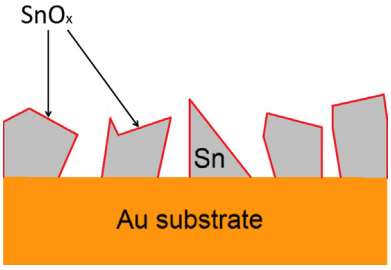

Fig. 5. Schematic picture of the electrodeposited tin oxide coated tin crystals on the gold substrate.

deposit did not fully coat the entire surface of the gold substrate. This is summarized in Fig. 5, which shows a schematic figure of what the deposited films looked like based on the characterization results.

3.3. *Electrochemical behavior in lithium-ion batteries*

The electrodeposited tin/tin oxide coatings were further characterised as anodes in pouch cell based lithium-ion batteries containing lithium counter electrodes. To study the different electrochemical processes (i.e., the conversion and alloy formation reactions described by Reactions 1 and 2) these experiments were carried out using CV with different potential windows at a scan rate of 1 mV/s, as described in more detail below.

3.3.1. *Cyclic voltammetric scans up to 3.0 V vs.* Li^+/Li

Cyclic voltammograms recorded for a tin sample coated with a native (i.e., about 6 nm thick) tin oxide film between 0.05 and 3.0 V and 0.9 and 3.0 V vs. Li^+/Li, respectively, are shown in Fig. 6. All voltammograms were recorded in the cathodic direction starting from the open circuit potential (OCP) of the battery, i.e., 2.4 V vs. Li^+/Li in the present case. It should, however, be pointed out that the OCP value was found to be as low as 0.7 V vs. Li^+/Li in some cases due to a relatively fast self-discharge caused by the small amounts of tin oxide present on the electrodes. The voltammograms in Fig. 6a are dominated by the reduction peaks at potentials lower than about 0.8 V vs. Li^+/Li and the oxidation peaks at potentials between 0.2 and 1.2 V vs. Li^+/Li. These peaks are generally assigned to lithium tin alloy formation and the oxidation of this alloy, respectively [6,14]. In Fig. 6a it can, however, also be seen that there was a rapid increase in the cathodic current at potentials below about 0.2 V vs. Li^+/Li which suggests the presence of alloying between gold and lithium as has previously been described in the literature. [35–37] The reason for this interference is the fact that the gold surface was not completely covered by the tin deposit as is seen in Fig. 1. This hypothesis is supported by the corresponding results obtained with a pure gold substrate (see the supporting information). These findings clearly demonstrate that the cathodic current at potentials below about 0.2 V vs. Li^+/Li mainly was due to the formation of a lithium gold alloy and that the oxidation of the latter alloy gave rise to the oxidation peaks between about 0.4 and 0.7 V vs. Li^+/Li. Although the presence of these reduction and oxidation peaks due to the lithium gold alloy complicates the interpretation of the voltammograms these peaks are still mainly separated from the peaks due to the lithium tin alloy. This clearly shows the advantage of using a gold substrate in the electrodeposition of tin materials to be used in fundamental studies of the electrochemical performance of tin based materials in lithium-ion batteries.

In Fig. 6a, there is, however, no sign of a SnO_2 reduction peak on the first cycle. This may initially appear to be puzzling as the reduction of SnO_2 as well as that of SnO (both yielding tin nanoparticles in a matrix of Li_2O according to Reaction 1) thermodynamically should

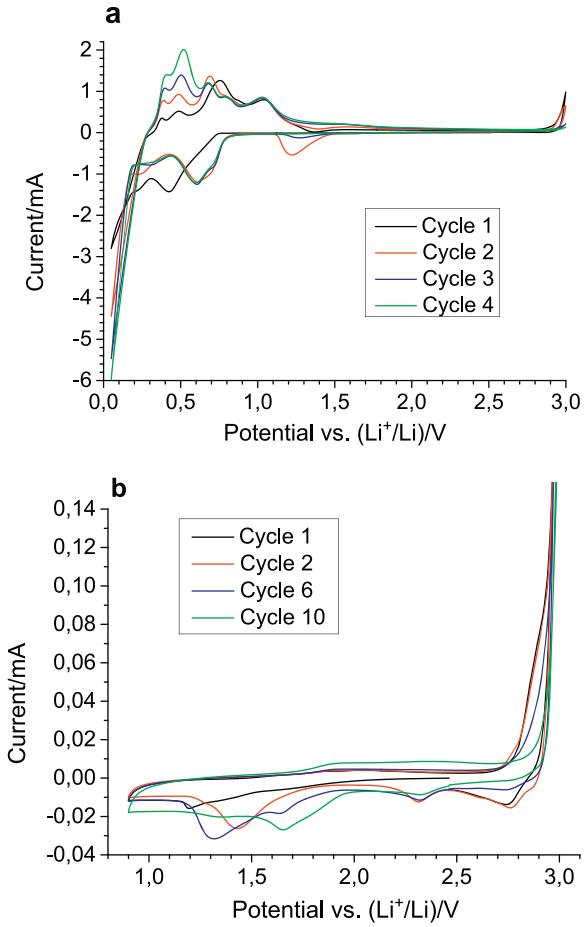

Fig. 6. Cyclic voltammograms recorded for native tin oxide coated samples cycled vs. lithium between a) 0.05 and 3 V vs. Li^+/Li and b) 0.9 and 3 V vs. Li^+/Li.

take place at about 1.6 V vs. Li^+/Li. A reduction peak at about 1.2 V vs. Li^+/Li was, on the other hand clearly seen on the second cycle most likely as a result of the oxidation taking place at about 3.0 V vs. Li^+/Li on the first anodic scan. Both the reduction peak at about 1.2 V vs. Li^+/Li and the oxidation at about 3.0 V vs. Li^+/Li, however, practically disappeared upon further cycling. The absence of a SnO_2 reduction peak on the first scan in Fig. 6a is, however, not unexpected since the amount of tin oxide present within the native tin oxide layer was very small and since the SnO_2 reduction on the first scan most likely was distributed over a relatively large potential range (see below). It is consequently difficult to study the conversion reaction in the presence of the alloying reaction for tin based electrodes covered with only a thin native layer of SnO_2. The presence of a tin oxide layer is, nevertheless, in good agreement with the OCP value of 2.4 V vs. Li^+/Li found at the start of the experiment.

As has been discussed by many authors [8–11], an SEI layer should be formed on the electrode at least in the potential region where the alloy formation reaction takes place. Reduction peaks observed between 1.2 V and 1.5 V vs. Li^+/Li have, however, sometimes also been ascribed to electrolyte decomposition yielding SEI formation. [12,13,21,47–50] In Fig. 6a, there is, nevertheless, no reduction peak which immediately can be ascribed to the formation of an SEI layer. This suggests that the current associated with this reaction likewise could have been too small to be seen in the presence of the lithium tin alloy formation reaction. This hypothesis can be further supported by estimating the expected SEI current for an assumed 100 mV wide SEI peak based on a 20 nm thick SEI layer, an SEI density of 2 g/cm^3 and a molecular mass of the SEI forming compounds of 150 g/mol. For a two-electron reduction process and an electroactive area of about 3.3 cm^2 (see below), an average cathodic current due to the SEI formation of about 0.13 mA would then be expected. Analogously, the expected average reduction current due to the reduction of a 6 nm thick SnO_2 layer would be of the order of 0.09 mA assuming a 400 mV wide reduction peak (see below). These currents are clearly small compared to the currents due to the alloy formation which explains why the SnO_2 reduction and the SEI formation reduction peaks cannot be seen in Fig. 6a. The peaks seen below about 2.5 V vs. Li^+/Li in Fig. 6a consequently mainly correspond to the electrochemical reactions associated with the formation and oxidation of the lithium tin alloy and the formation and oxidation of a lithium gold alloy, respectively.

To be able to study the conversion reaction (i.e., Reaction 1) cyclic voltammograms were further recorded between 0.9 V and 3.0 V vs. Li^+/Li as is shown in Fig. 6b. By comparing the current scales in Figs. 6a and b it is immediately evident that the SnO_2 reduction current would indeed be difficult to detect in the presence of the alloy formation reaction. From Fig. 6b, it is also clear that the reduction of the native tin oxide layer took place in a rather wide potential window on the first cycle while a more well-defined tin oxide reduction peak was seen on the subsequent cycles. In analogy with the behavior seen in Fig. 6a, the magnitude of the oxidation current at about 2.9 V vs. Li^+/Li decreased on the subsequent cycles. This indicates that the formed oxidation product could not be fully reduced on the subsequent cathodic scan. A small reduction peak at approximately 2.75 V vs. Li^+/Li, which probably is directly coupled to the oxidation peak at 2.9 V vs. Li^+/Li, can also be seen for the first two scans in Fig. 6b. On the tenth cycle, a broad reduction peak at about 1.7 V vs. Li^+/Li (which most likely is coupled to the broad oxidation wave seen at potentials larger than about 1.75 V vs. Li^+/Li) can instead be seen. These results suggest that the oxidation at 2.9 V involves the formation of an oxidation product which at least initially can undergo partial reduction at about 2.75 V vs. Li^+/Li and that the reduction peaks seen at 1.7 to 1.3 V vs. Li^+/Li on the second and subsequent scans involve Reaction 2. The latter would be in agreement with the standard potential of about 1.6 V vs. Li^+/Li previously mentioned. The fact that the reduction peak charge was 16 mC for the second cycle and 21 mC for the tenth cycle whereas the corresponding oxidation charges were 16 and 18 mC also demonstrates the presence of an essentially reversible redox reaction in this potential window.

3.3.2. *Cyclic voltammetric scans up to 2.5 V vs.* Li^+/Li

As is seen in Fig. 7a, the first cycle voltammogram recorded with a native tin oxide film on the tin crystals between 0.9 and 2.5 V vs. Li^+/Li exhibited a reduction peak at about 1.6 V vs. Li^+/Li, a broad reduction peak at approximately 1.1 V vs. Li^+/Li and two broad oxidation peaks at about 1.8 and 2.2 V vs. Li^+/Li. In this case it is reasonable to assume that the reduction peaks at 1.1 and 1.6 V vs. Li^+/Li were due to the reduction of SnO_2 and a thin layer of SnO formed on top of the SnO_2 layer during self-discharge. The broad oxidation peaks may consequently be ascribed to the formation of SnO and SnO_2 which according to thermodynamics should be formed at roughly the same potential (i.e., about 1.6 V vs. Li^+/Li). One problem here is that the oxides formed would act as passivating layers which most likely explains the drawn-out oxidation peaks as well as the significantly smaller oxidation charge compared to the reduction charge on the first cycle. In Fig. 7a, the first and tenth cycle reduction charges in Fig. 7a were 35 and 12 mC, respectively, while the corresponding oxidation charges were 8 and 10 mC, respectively. The tenth cycle charges were thus only about half of those obtained when cycling between 0.9 and 3.0 V vs. Li^+/Li

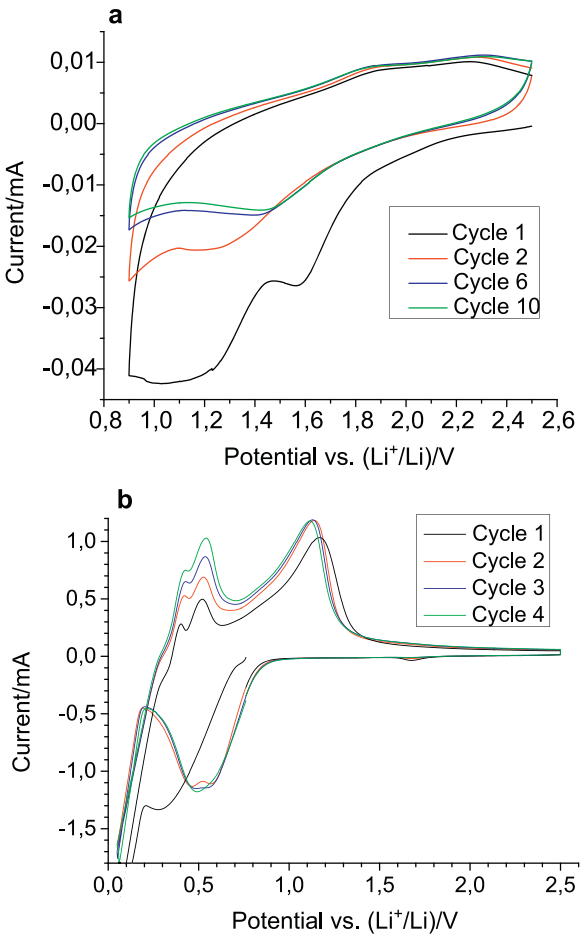

Fig. 7. Cyclic voltammograms recorded for native tin oxide coated samples cycled vs. lithium between a) 0.9 and 2.5 V vs. Li^+/Li and b) 0.05 and 2.5 V vs. Li^+/Li.

(see Fig. 6) supporting the hypothesis that the formation of SnO_2 on the anodic scan takes place within a relatively wide potential window. The latter is, however, not unexpected as this effect is well-known [51–53] for metals forming passive layers.

Fig. 7b depicts voltammograms obtained with native oxide coated films cycled between 0.05 V and 2.5 V vs. Li^+/Li, i.e., in a potential window including also the tin and gold alloying reactions. While these voltammograms generally are very similar to those seen in Fig. 6a, some small differences exist. In Fig. 7b, a small reduction peak, which disappears upon further cycling, is, for example, seen at about 1.7 V vs. Li^+/Li on the first scan. This small reduction peak is therefore likely to be due to the reduction of SnO and SnO_2 in reasonable agreement with the data in Fig. 7a. The shapes of the alloy formation and dealloying peaks on the first cycle also differ somewhat compared to those seen in Fig. 6a. This probably reflects differences in the conditions affecting the nucleation of the lithium tin alloy for the different samples since it is well-known [28,29,54,55] that the electrodeposition of metals is very sensitive to changes in the experimental conditions. The reduction peak at about 1.2 V vs. Li^+/Li seen on the second cycle in Fig. 6a (which most likely is due to SnO_2 reduction) is clearly missing in Fig. 7b which supports the hypothesis that the latter peak is coupled to the oxidation seen above 2.8 V vs. Li^+/Li in Fig. 6a. In Fig. 7b the presence of a continued oxidation at potentials larger than 1.3 V vs. Li^+/Li is likewise clearly seen which could either stem from the dealloying reaction (i.e., oxidation of the lithium within the alloy), the oxidation of elemental tin, or a combination of both reactions. A closer look at the voltammograms shows that the current remained anodic even on the following cathodic scan (at least up to about 1.7 V vs. Li^+/Li) suggesting that the complete oxidation of the lithium within the alloys is relatively slow (and most likely mass transport controlled) process. The latter effect explains some of the problems associated with the detection of the tin oxide reduction currents in Fig. 6a and 7b.

To investigate the electrochemical performance of samples coated with thicker (i.e., 12 and 24 nm thick) tin oxide layers, analogous cyclic voltammetric experiments were carried out with samples which had undergone electrochemical anodization involving linear sweep voltammetry to +0.8 and +1.0 V vs. $Ag/AgCl$, respectively (see experimental section). Although the shapes of the corresponding cyclic voltammograms (see the supporting information) were generally very similar to those depicted in Fig. 7a, the reduction and oxidation charges were found to increase with growing oxide layer thickness. This demonstrates that these peaks were indeed due to redox reactions involving the tin oxide layer. A comparison of the reduction and oxidation charges for the different samples cycled between 0.9 and 2.5 V vs. Li^+/Li further showed that these charges were proportional to the oxide layer thickness. In all cases, a significantly larger first cycle reduction charge (compared to those obtained on the subsequent cycles) was found indicating an incomplete formation of SnO_2 on the subsequent anodic scan. As already mentioned, the reduction on the first cycle should involve SnO_2 (in addition to some SnO formed via self-discharge) while SnO and SnO_2 can be expected to be formed on the subsequent anodic scan. A reduction peak corresponding to the small SnO peak seen at about 1.6 V on the first scan in Fig. 7a (for the native oxide) was, on the other hand, not seen for the thicker SnO_2 layers most likely as such a peak would be difficult to detect in these cases due to the larger reduction current obtained for these samples (a small reduction peak at about 1.7 V vs. Li^+/Li could in fact be seen for the 12 nm thick film). The samples anodized at +0.8 and +1 V vs. $Ag/AgCl$ exhibited first reduction charges of about 70 and 149 mC, respectively, while the corresponding reduction charges on the tenth cycle were 26 and 79 mC for the samples anodized at +0.8 and +1.0 V, respectively. The oxidation charges, on the other hand, increased from 20 to 24 mC for the sample anodized at +0.8 V vs. $Ag/AgCl$ and from 57 to 77 mC for the sample anodized at +1.0 V vs. $Ag/AgCl$, respectively. These findings hence show that the tenth cycle reduction charges only corresponded to about 37 and 53 % of the first cycle charges for the samples anodised at +0.8 and +1.0 V vs. $Ag/AgCl$, respectively. As the corresponding value was about 35 % for the native oxide layer the present results suggest that the reformation of SnO_2 could become more facile as the thickness of the SnO_2 layer increases when cycling between 0.9 and 2.5 V vs. Li^+/Li.

By assuming that the reduction seen on the first cycle (when scanning between 0.9 and 2.5 V vs. Li^+/Li) were indeed due to the reduction of SnO_2 it becomes possible to calculate the expected reduction charges for the different SnO_2 thicknesses. Such a calculation (based on a geometric electrode area of 1.77 cm^2, a SnO_2 density of 6.95 g/cm^3, a SnO_2 molar mass of 150.71 g/mol and a four-electron reduction process according to Reaction 1) indicates that the obtained reduction charges for 6, 12 and 24 nm thick SnO_2 layers should be about 19, 38 and 76 mC, respectively. These charges are, however, somewhat smaller than the experimental values (i.e., 35, 70 and 149 mC). The latter can most likely be explained by the presence of a surface roughness effect (see the SEM image in Fig. 1b) of about 1.9 yielding an electroactive area of about 3.3 cm^2 for all three samples. As this surface roughness factor is reasonable considering that the surface coverage of the tin coating was significantly less than 100 %, this calculation further supports the hypothesis that the SnO_2 layer is fully reduced according to Reaction 1 on the first reduction cycle.

A comparison of the cyclic voltammograms obtained between 0.05 and 2.5 V vs. Li^+/Li for the three different SnO_2 thicknesses (i.e., 6, 12 and 24 nm, see Fig. 7b and supporting information), on

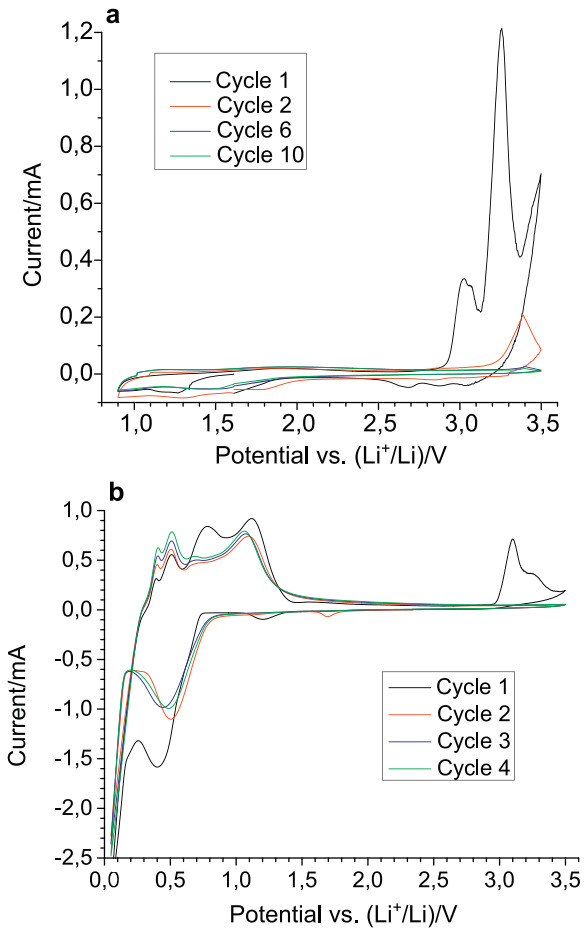

Fig. 8. Cyclic voltammograms recorded for native tin oxide coated samples cycled versus lithium between a) 0.9 and 3.5 V vs. Li^+/Li and b) 0.05 and 3.5 V vs. Li^+/Li.

the other hand, clearly showed that the reduction and oxidation charges associated with the lithium tin alloy and lithium gold alloy formation and the oxidation of the alloys were practically independent of the thickness of the SnO_2 layer. This result is, however, not unexpected as the SnO_2 layers on the Sn crystals were fully reduced to elemental tin at potentials of about 1.0 V vs. Li^+/Li as discussed above.

3.3.3. *Cyclic voltammetric scans up to 3.5 V vs.* Li^+/Li

To further study the oxidation reaction taking place above about 2.8 V vs. Li^+/Li cyclic voltammograms were also recorded between 0.9 and 3.5 V vs. Li^+/Li as well as between 0.05 and 3.5 V vs. Li^+/Li as indicated in Fig. 8. In Fig. 8a, it is seen that at least two oxidation peaks were obtained on the first scan at about 3.0 and 3.2 V vs. Li^+/Li, respectively, and that the reduction charge on the preceding cathodic scan was very small compared to the first cycle oxidation charge. Oxidation peaks above 2.8 V vs. Li^+/Li, although exhibiting a different peak size distribution, were also seen after a cathodic scan to 0.05 V vs. Li^+/Li as is seen in Fig. 8b. Based on the first cycle voltammograms in Fig. 8a it is immediately evident that the oxidation must have involved a further oxidation of the surface of the tin crystals. Due to the lack of an oxygen source in the electrolyte it is also clear that the oxidation could not have given rise to additional SnO_2. Although traces of water certainly were present in the electrolyte these are unlikely to have acted as an oxygen source since the water should have been irrversibly reduced on the preceeding cathodic scan. This reduction should have resulted in the formation of O^{2-} which then should have reacted with the electrolyte to yield a contribution to the SEI layer. It is also difficult to ascribe the large oxidation peaks to the formation of additional tin oxide as the thermodynamically based potentials for the oxidation of tin to tin(II) oxide and tin(IV) oxide, respectively both are about 1.6 V vs. Li^+/Li. It is, on the other hand, reasonable to assume that the oxidation could have involved oxidation on tin yielding SnF_2, particularly as fluoride ions are well-known to be present in $LiPF_6$ containing electrolytes. These can stem from selfdegradation of the electrolyte, but also from reactions with trace amounts of water. [56–58] Although it was not possible to calculate the standard potential for the conversion reaction involving SnF_2, due to a lack of a ΔG_0 value for SnF_2, the corresponding values for $SnBr_2$ (i.e., 2.2 V vs. Li^+/Li) and $SnCl_2$ (i.e., 2.5 V vs. Li^+/Li) could be calculated based on readily available ΔG_0 values. [59] The latter values indicate that the standard potential for the SnF_2 reaction should be of the order of 3 V vs. Li^+/Li. The standard potential for the reaction $SnF_4 + 2e - \rightleftharpoons SnF_2 + 2F^-$ has also been reported to be 3.15 V vs. Li^+/Li. [60] According to these data it is hence reasonable to assume that the oxidation seen at potentials above about 2.8 V vs Li^+/Li mainly stems from the oxidation of tin to SnF_2.

As is also evident from Fig. 8, the majority of the generated oxidation product (i.e., mainly SnF_2) could, however, not be reduced on the subsequent scans. The oxidation charge in Fig. 8a was thus 356 mC while the charge of the reduction charges of the preceding and subsequent reduction scans were 34 and 59 mC, respectively. This phenomenon is, however, readily explained by the fact that SnF_2 which was formed underneath a layer of SnO and SnO_2 in analogy with the behavior for the successive formation of other metal oxides. [61] On the subsequent cathodic scan it will hence be difficult to reduce the SnF_2 completely as this requires the transport of lithium ions through the tin oxide layer on top of the SnF_2 layer. This also explains why the formation of SnF_2 does not interfere very much with the electrochemical reactions involving the tin oxides (see Fig. 6b and 8a). The cathodic current between about 3.2 and 2.5 V vs. Li^+/Li can hence be ascribed to a partial reduction of the SnF_2 yielding tin nano-particles in a matrix of LiF as indicated in Reaction 7 below.

$$2Li^+ + 2e^- + SnF_2 \rightleftharpoons 2LiF + Sn \quad (7)$$

Another factor that could contribute to the poor reversibility for the SnF_2 reaction is that the generated LiF has been reported to be very stable [62–64] which means that the reformation of SnF_2 could be more difficult than that of SnO_2 or SnO.

As already explained, the reduction peak at about 1.2 V vs. Li^+/Li in Fig. 8b most likely stems from the reduction of SnO_2 according to Reaction 1 whereas the reduction peak at about 1.5 V vs. Li^+/Li on the second cycle in the same figure can be ascribed to SnO reduction. The reduction peak seen at about 1.2 V vs. Li^+/Li on the second cycle in Fig. 6a thus suggests that oxidation to SnO_2 required scans to potentials above 2.8 V vs. Li^+/Li.

The corresponding voltammograms recorded between 0.9 and 3.5 V vs. Li^+/Li for the two electrodes with thicker SnO_2 layers also exhibited large oxidation peaks at potentials above about 3.0 V (see the supporting information). The oxidation charges were, however, significantly smaller (i.e., 144 and 112 mC) for the 12 and 24 nm SnO_2 films when compared to the 356 mC obtained for the native SnO_2 film. This is not unexpected since the presence of a thicker oxide layer should make it more difficult to oxidize the underlying tin. For the 12 and 24 nm thick SnO_2 films, there were no signs of any oxidation peak on the subsequent anodic scans or any reduction peaks at 3.0 and 2.6 V vs. Li^+/Li on the second cathodic scan as for the native (i.e., 6 nm thick) SnO_2 film. A well-defined reduction peak at about 1.4 V vs. Li^+/Li and a broad oxidation peak between 1.7 and 2.7 V vs. Li^+/Li were, on the other hand, also seen on the subsequent cycles. The first and tenth cycle reduction charges for the 12 nm thick oxide film were 72 and 59 mC while the corresponding values for the 24 nm thick film were 123 and 81 mC, respectively.

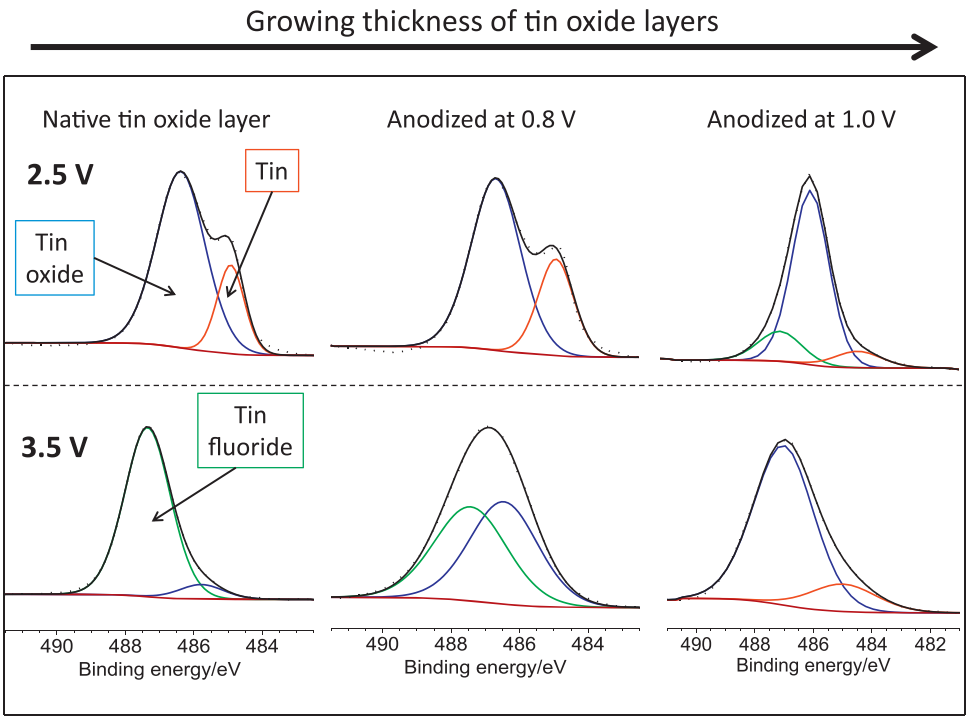

Fig. 9. XPS spectra with curves fitted to the $3d\frac{5}{2}$ tin peak for different tin oxide layer thicknesses after cycling to 2.5 V and 3.5 V vs. Li^+/Li, respectively.

These values are in reasonably good agreement with the expected first cycle reduction charges of 72 and 144 mC for the anodized films (since the experimental values correspond to 100 % and 85 % of the theoretical values for the two anodized films). In addition, the tenth cycle reduction charges obtained when cycling between 0.9 and 2.5 V vs. Li^+/Li corresponded to 82 % (12 nm thick film) and 65 % (24 nm thick film) of the first cycle reduction charges. As these values are larger than those of 37 % and 53 % obtained when cycling between 0.9 and 2.5 V vs. Li^+/Li, it is clear that a larger fraction of the initially present SnO_2 was reformed upon cycling to 3.5 V than to 2.5 V vs. Li^+/Li. This is in good agreement with the general behavior associated with the formation of passivating layers on metals [51–53].

3.4. XPS characterization of electrodes cycled to 2.5 V or 3.5 V vs. Li^+/Li

To facilitate the interpretation of the electrochemical experiments, XPS spectra were also recorded after having cycled the electrodes from the OCP (i.e., about 2.4 V vs. Li^+/Li) down to 0.9 V and then up to either 2.5 V or 3.5 V vs. Li^+/Li for all tin oxide layer thicknesses to study the composition of the electrodes at the respective potentials. As is seen in Figs. 9, 10 and 11, the surface characterization, which thus was carried out on the first oxidation cycle, focused mainly on tin, oxygen and fluorine. It was, however, also found that the carbon spectra exhibited the typical peaks commonly associated with the presence of an SEI layer formation although this will not be discussed further [65–67].

XPS profiles were recorded and fitted to the Sn $3d\frac{5}{2}$, F 1s and O 1s XPS spectra (after 2.5 V or 3.5 V vs. Li^+/Li) which are shown in Figs. 9, 10 and 11. At 2.5 V vs. Li^+/Li, the Sn $3d\frac{5}{2}$ spectra exhibited mainly contributions from elemental tin and SnO (see references [68] for more information regarding the tin oxide peak assignment) whereas an additional peak, most likely due to SnF_2 could be seen at higher binding energies after cycling to 3.5 V vs. Li^+/Li. As is seen in Fig. 9, the relative contributions for the different components depended on the thickness of the SnO_2 layer originally present on the electrode. For the thickest oxide there was a relative small contribution from elemental tin and a large contribution from tin oxide (i.e., SnO) at 2.5 V vs. Li^+/Li as could be expected. At this potential, a peak most likely due to SnO_2 could also be seen for the latter sample but not for the other two samples. These results hence indicate that mainly SnO was present on the electrode surface after scanning up to 2.5 V vs. Li^+/Li. The XPS spectra for the electrodes cycled up to 3.5 V vs. Li^+/Li were less straightforward to interpret probably due to a lower conductivity of the surfaces of these samples. It is therefore not immediately clear if the peak at about 487.2 to 487.5 eV, seen for all three electrodes, should be ascribed to SnF_2 or SnO_2 and what the peak at about 486.5 eV stemmed from. The peak at about 484.9 eV seen for the thickest oxide appears to stem from elemental tin although it is not clear why this would be the case as the contribution from elemental tin should be the smallest for this sample.

The F 1s spectra depicted in Fig. 10 indicate that LiF and some $LiPF_6$ were present on the surface of the samples cycled to 2.5 V vs. Li^+/Li as well as on the thickest oxide sample cycled to 3.5 V vs. Li^+/Li. This is not surprising as these components generally are found for electrodes exposed to $LiPF_6$ containing electrolytes. [25,56,57,69,65,67] More importantly, a component, probably stemming from SnF_2 was seen for the electrodes with the native and 12 nm thick oxides but not for the sample with the thickest oxide after cycling to 3.5 V vs. Li^+/Li. These results hence demonstrate that while SnF_2 is unlikely to form at 2.5 V vs. Li^+/Li, but it can most likely be formed during a scan to 3.5 V vs. Li^+/Li.

The O 1s spectra in Fig. 11 clearly show that tin oxide was present on the surface of all samples and that the overall tin oxide contribution increased when cycling to 3.5 rather than 2.5 V vs. Li^+/Li. It is also evident that there was a shift towards higher binding energies for the tin oxide peak when going from 2.5 to 3.5 V vs. Li^+/Li, most likely indicating that SnO and SnO_2 dominated at 2.5 and 3.5 V vs. Li^+/Li, respectively. Since the O 1s spectra indicate that lithium carbonate was present on the surface of the samples it can also be concluded that SEI formation can take place during cycling to 0.9 V vs. Li^+/Li although it should be mentioned that a reduction of the solvent at the lithium counter electrode cannot be excluded.

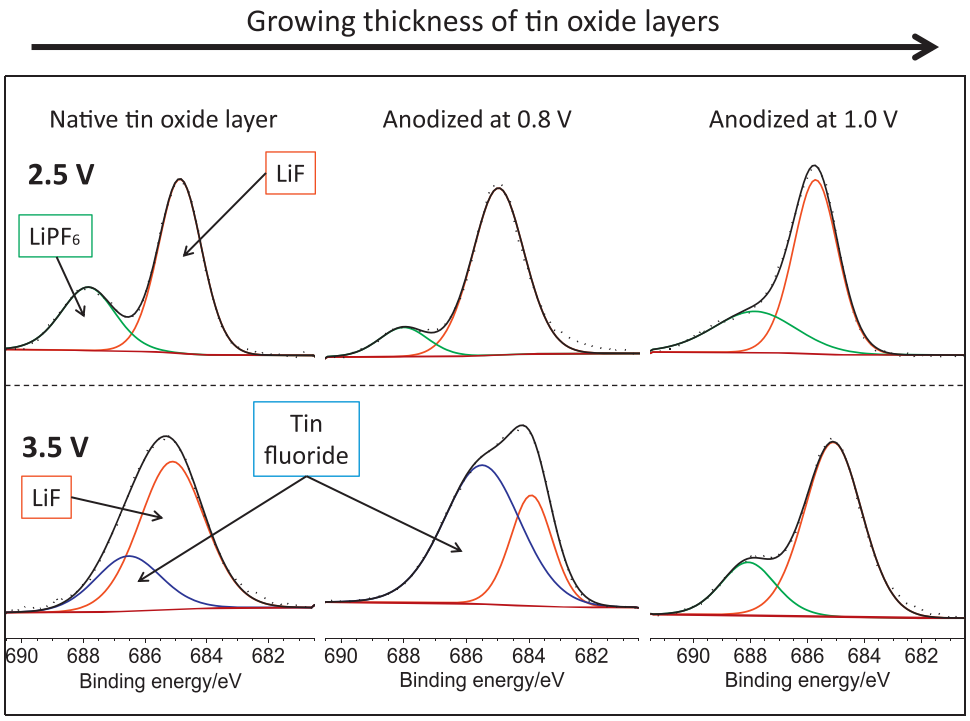

Fig. 10. XPS spectra with curves fitted to the 1s fluorine peak for different tin oxide layer thicknesses after cycling to 2.5 V and 3.5 V vs. Li^+/Li, respectively.

3.5. *SEM characterization of electrodes cycled to 2.5 V or 3.5 V vs.* Li^+/Li

As is seen from the SEM images in Fig. 12, which were taken after having cycled electrodes with the native oxide to 2.5 and 3.5 V vs. Li^+/Li, respectively, the deposited oxide coated tin crystals were still clearly seen after cycling to 2.5 V vs. Li^+/Li. This SEM image is thus very similar to that (see Fig. 1) taken prior to the cycling. From the SEM image taken after cycling to 3.5 V vs. Li^+/Li it is, on the other hand, immediately evident that cycling to this potential gave rise to a completely different surface as the crystals seen after cycling to 2.5 V vs. Li^+/Li no longer can be seen in the SEM image. Although some cracks, which might originate from a volume expansion effect, can be seen on the surface there is no sign of any loss or detachment of material. Based on the SEM images it can thus be concluded that the surface morphology changed dramatically

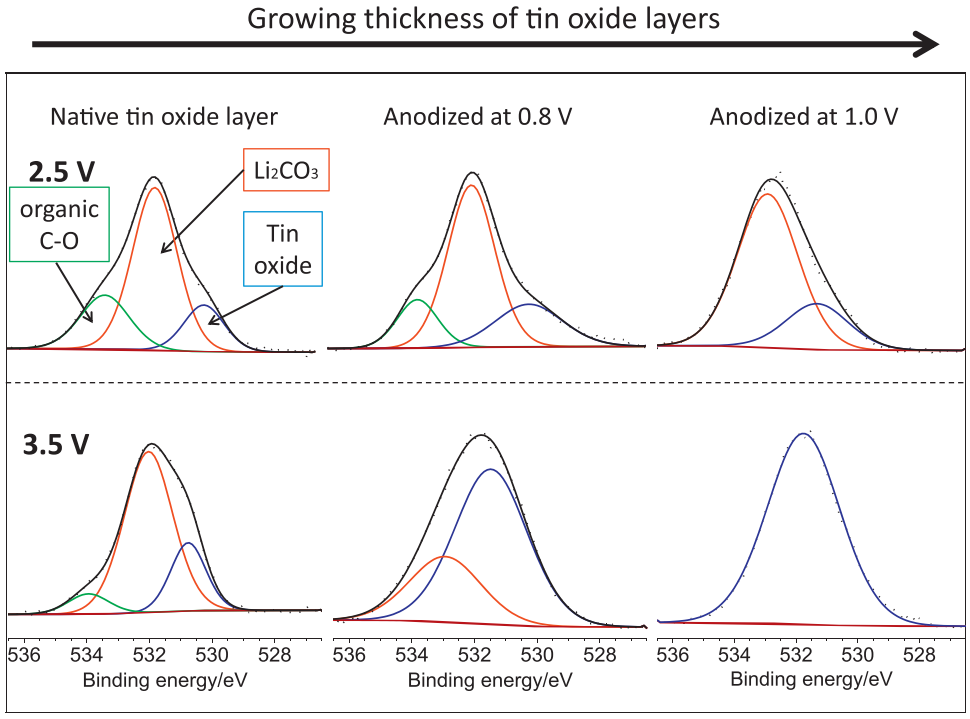

Fig. 11. XPS spectra with curves fitted to the 1s oxygen peak for different tin oxide layer thicknesses after cycling to 2.5 V and 3.5 V vs. Li^+/Li, respectively.

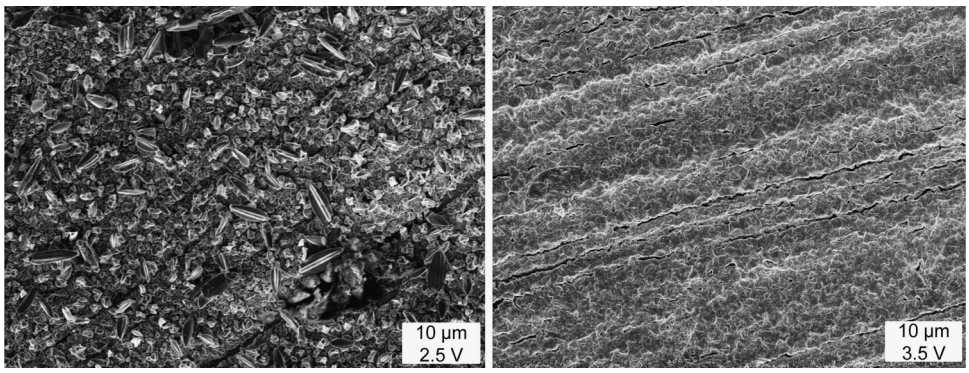

Fig. 12. SEM images of the native oxide coated samples cycled to 2.5 V and 3.5 V vs. Li^+/Li, respectively.

when the electrode was cycled from 2.5 to 3.5 V vs. Li^+/Li while the samples cycled to 2.5 V vs. Li^+/Li and un-cycled samples exhibited very similar morphologies. The dramatic change in the morphology of the sample can therefore be ascribed to the formation of SnF_2 at potentials higher than 2.8 V vs. Li^+/Li.

3.6. *The electrochemical behavior of* SnO_2 *coated Sn electrodes*

The electrochemistry of the present SnO_2 coated tin crystals which were electrodeposited on gold substrates to avoid significant interactions with the substrate can conveniently be discussed based on the three different types of electrochemical reactions presented above, i.e., the lithium tin alloy reaction, the tin oxide conversion reactions and the tin(II) fluoride conversion reaction. These reactions will therefore be discussed separately in the paragraphs below.

The formation and oxidation of the lithium tin alloy. Based on the results in Figs. 6a, 7b and 8b, it is clear that the reduction and oxidation peaks at potentials below about 1.2 V vs. Li^+/Li can be ascribed to the formation and oxidation of a lithium tin alloy and a lithium gold alloy and that no reduction peak due to the formation of an SEI could be seen as the current associated with such a process would be too small to detect in the presence of the alloy formation reaction. An SEI is naturally still formed in this potential region even though it cannot be seen in the voltammograms. The data also show that lithium gold alloy formation takes place at potentials below about 0.2 V vs. Li^+/Li in good agreement with previous findings. [35–37] This effect stems from the fact that the surface coverage of tin on the gold substrate was significantly smaller than 100 % as is seen in Fig. 1.

Analogously it is clear that the lithium gold alloy is oxidized at potentials between 0.4 and 0.7 V vs. Li^+/Li while the lithium tin alloy gives rise to the oxidation peak at about 0.7 to 1.0 V vs. Li^+/Li. As is clearly seen from Figs. 6a, 7b and 8b the oxidation of the lithium tin alloy (and analogously also the lithium gold alloy) continued to contribute to the current at least up to a potential of 2.5 V vs. Li^+/Li on the anodic scan. This can be readily explained by the fact that the oxidation of the alloy starts at the surface of the electrode and continues inwards which gives rise to a growing layer of elemental tin on top of the remaining alloy. Since the lithium must diffuse through this layer of tin to get to the surface this phenomenon gives rise to an extended and in many cases probably also incomplete oxidation process. Since the formation of the alloy (which likewise takes place on the tin surface) results in the formation of an alloy which gradually spreads inwards there is no corresponding slow step during the deposition of the alloy or the subsequent deposition of lithium on top of the alloy. This means that there is a fundamental electrochemical difference between the reactions involving alloy formation and oxidation of the alloy which should be seen for all metals forming alloys with lithium. This effect will thus generally give rise to too small oxidation charges when compared to the reduction charges, i.e., coulombic efficiencies lower than 100 %.

The conversion reactions involving SnO_2 *and SnO*. The present results clearly show that it is possible to fully reduce SnO_2 films with thicknesses of up to 24 nm within a potential region from about 1.8 V to 1.0 V vs. Li^+/Li, but that the corresponding formation of SnO_2 on the subsequent anodic scan is incomplete even for scans up to 3.5 V vs. Li^+/Li. The problem is thus not the reduction of the SnO_2 but the oxidation involving the reformation of the SnO_2. The experimental results also show that it is unlikely that the irreversible electrochemical behavior of SnO_2 is coupled to the volume expansions associated with the conversion reaction.

Based on the voltammetric and XPS results *SnO* appears to be the dominating oxide for potentials between about 1.7 to 2.5 V vs. Li^+/Li while an increasing fraction of SnO_2 is formed upon scanning to 3.0 V and 3.5 V vs. Li^+/Li. The problems associated with the reformation of SnO_2 is most likely due to the fact that the formation of the oxides gives rise to a growing passivating layer which makes additional formation of SnO_2 more and more difficult. The latter is not surprising as the formation of SnO_2 (i.e., $Sn + 4Li_2O \rightleftharpoons SnO_2 + 4Li^+ + 4e^-$) requires that lithium ions can be transported through the growing oxide layer to maintain electroneutrality. There is, on the other hand, no corresponding slow step during the reduction of the SnO_2 since this reaction gives rise to tin nanoparticles in a matrix of Li_2O. This means that the required mass transport of lithium ions should be relatively fast. In analogy with the alloy formation reaction there is hence an asymmetry with respect to the reduction and oxidation steps of the conversion reaction.

As mentioned in the introduction, there are several reports demonstrating a partial reversibility of the conversion reaction for SnO_2 nanoparticles. [38,70,71] In many of the reports the partial reversibility has been ascribed to the small size of the particles and the presence of other phases like copper or carbon. Since the present experiments were carried out with micrometer sized tin crystals coated with up to 24 nm thick SnO_2 films in the absence of any additives it is reasonable to assume that the observed reversibility was due to the relatively thin SnO_2 coatings. Since Chouvin et al. [17,18] observed partial reversibility for *SnO* it is even possible that nanosized tin oxide particles or nanometer thick tin oxide layers may not be absolutely necessary at all. Based on the discussion above it is, however, evident that a full utilization of a sufficiently thick SnO_2 film or sufficiently large SnO_2 particles is unlikely on reasonable time scales.

Although Chouvin et al. [17,18] suggested that the alloy formation could interfere with $Sn-O$ interactions and lead to tin agglomeration when cycling to potential below 0.3 V vs. Li^+/Li and therefore disturb the reformation of tin oxide, no evidence for

such an effect have been found in the present study. It should, however, be pointed out that it was difficult to study the conversion reaction in the presence of the alloying reaction as the currents due to the latter reaction were significantly higher and therefore masked the currents associated with the conversion processes. Since the conversion reaction gives rise to tin nanoparticles in a Li_2O matrix and the subsequent alloy formation should convert the tin into a lithium tin alloy which still should be surrounded by Li_2O it is not immediately clear why the formation of the alloy would affect the reversibility of the SnO_2 conversion reaction.

The formation of tin(II) fluoride. As is seen in Figs. 6b and 8 large oxidation peaks due to the formation of SnF_2 could be seen when scanning to potentials higher than about 2.8 V vs. Li^+/Li. This oxidation did, however, not affect the reversibility of the SnO_2 conversion reaction significantly since the formation of the SnF_2 should have taken place below the tin oxides. The latter also explains the problems associated with the subsequent reduction of the SnF_2 (i.e., the conversion reaction involving SnF_2). Although it has been proposed that SnF_2 can be formed as a result of a degradation of the PF_6^- present in the electrolyte [25,56,57,69,65,67] it is not clear if this reaction involves PF_6^- ions or fluoride ions formed as a result of a previous degradation of the PF_6^-. Since the anions would need to migrate through the tin oxide layer during the formation of the SnF_2 the latter does seem less likely.

As discussed above, the scans to 3.5 V vs. Li^+/Li also facilitated the formation of SnO_2 which means that a layer containing SnO_2, SnO as well as SnF_2 most likely were present on the tin crystals after scanning to 3.5 V vs. Li^+/Li. This is partially supported by the XPS results which unfortunately were difficult to interpret for the 3.5 V vs. Li^+/Li case most likely due to the relatively low conductivity of the surface layers.

The extent of SnF_2 formation was marked lower for the anodized films which had thicker SnO_2 layers in good agreement with the explanation presented above. The presence of a thick tin oxide layer can likewise explain why no SnF_2 was seen in the XPS results for the thickest film at 3.5 V vs. Li^+/Li. Even though, there was a dramatic change in the morphology associated with the SnF_2 formation (the expected volume expansion when going from elemental tin to SnF_2 is about 210 % calculated from readily available density values [59]) this did not result in any significant loss of capacity for the SnO_2 conversion reaction. This further supports the conclusion that the reversibility problems associated with the SnO_2 (or the SnO) system do not originate from volume expansion effects.

It should also be mentioned that tin(II) fluoride (SnF_2) [62,63], tin lead fluoride ($PbSnF_4$) [72] as well as tin fluorophosphate ($Sn_3F_4PO_4$) [73] have also been studied as anode materials. For both SnF_2 and $Sn_3F_4PO_4$ a reduction yielding tin and LiF was reported to be present on the first cycles at a potential of about 1.6 V vs. Li^+/Li. [62] This could suggest that the reformation of the SnF_2 on the subsequent anodic scan was even more difficult than that for SnO_2. Connor et al. [63] even concluded that LiF generally is more chemically inactive than Li_2O.

4. Conclusions

The electrochemical reactions involving tin oxide coated tin electrodes in a lithium-ion battery have been studied in detail using electrodeposited tin crystals on a gold substrate. Since the electrodes did not contain any additives it was, with the help of XPS and SEM investigations, possible to ascribe practically all the reduction and oxidation peaks in the voltammograms to either tin oxide conversion reactions, lithium tin alloy formation/oxidation, or the formation and reduction of tin(II) fluoride. This improved electrochemical understanding of the SnO_2/Sn system is essential in the development of improved tin based electrodes for lithium-ion batteries.

It has been shown that SnO_2 electrodes used in lithium-ion batteries readily can undergo a conversion reaction to yield tin and Li_2O but that the formation of SnO_2 on the subsequent anodic scan is limited by the fact that the formed oxide acts as a passive layer. This means that a complete oxidation to SnO_2 most likely requires a large overpotential and long oxidation times. As has been demonstrated in the present work, it is, nevertheless, possible to obtain capacities corresponding up to about 80 % of that of the initial reduction charge by scanning up to 3.5 V vs. Li^+/Li. It can, therefore, be concluded that the reversibility problems for SnO_2 do not stem from volume expansion effects or the agglomeration of tin particles but rather the transport of lithium ions across a tin oxide layer of increasing thickness.

It can also be concluded that the formation of the lithium tin alloy is faster than the corresponding oxidation of the alloy since the latter process is limited by the diffusion of lithium through a layer of elemental tin with an increasing thickness. The results further indicate that lithium gold alloy formation takes place at potentials lower than about 0.2 V vs. Li^+/Li and that the oxidation of this alloy gives rise to an oxidation peak at about 0.3 to 0.4 V vs. Li^+/Li.

At potentials above about 2.8 V vs. Li^+/Li SnF_2 can form under the already existing tin oxide layer. This reaction gives rise to a major oxidation peak but practically no corresponding reduction peak most likely as a result of the problems associated with the required mass transport of lithium ions through the oxide layer. The formation of the SnF_2 layer does, however, not affect the capacity associated with the SnO_2 reactions nor that coupled to the lithium tin alloy reactions.

It, consequently, has been demonstrated that the oxidation of the lithium tin alloy and that yielding SnO_2 from elemental tin and Li_2O are significantly slower reactions than the formation of the alloy and the reduction of SnO_2. The reduction of the SnF_2 formed at potentials higher than about 2.8 V vs. Li^+/Li is likewise significantly slower than the oxidation generating SnF_2. These phenomena, which all can be explained based on the electrochemical conditions connected with the different reactions, are most likely also observed in many other systems of interest to lithium-ion batteries. This improved understanding should hence significantly facilitate the development of new improved electrodes for lithium-ion batteries.

Acknowledgements

The authors would like to thank Maria Hahlin for help regarding the XPS measurements and analysis of XPS data. This work was funded by the Swedish Foundation for Strategic Research (SSF).

Appendix A. Supplementary Data

Supplementary data associated with this article can be found, in the online version, at http://dx.doi.org/10.1016/j.electacta.2015.02.150.

References

[1] W. Zhang, J. Power Sources 196 (2011) 13–24.
[2] M. Palacin, Chem. Soc. Rev. 38 (2009) 2565–2575.
[3] A. Kamali, D. Fray, Rev. Adv. Mater. Sci. 27 (2011) 14–24.
[4] D. Deng, M. Kim, J. Lee, J. Cho, Energy Environ. Sci. 2 (2009) 818–837.
[5] J. Tirado, Materials Science & Engineering, R 40 (2003) 103–136.
[6] I. Courtney, J. Dahn, J. Electrochem. Soc. 144 (1997) 2045–2052.
[7] S. Chou, J. Wang, H. Liu, S. Dou, Electrochem. Commun. 11 (2009) 242–246.
[8] H. Li, X. Huang, L. Chen, Electrochem. Solid-State Lett. 1 (1998) 241–243.
[9] M. Winter, Z. Phys. Chem. 223 (2009) 1395–1406.
[10] K. Ehinon, S. Naille, R. Dedryvere, P.-E. Lippens, J.-C. Jumas, D. Gonbeau, Chem. Mater. 20 (2008) 5388–5398.

[11] D.-T. Shieh, J. Yi, K. Yamamoto, M. Wada, S.T.T. Sakai, J. Electrochem. Soc. 153 (2006) A106–A112.
[12] I. Lucas, E. Pollak, R. Kostecki, Electrochem. Commun. 11 (2009) 2157–2160.
[13] I. Lucas, J. Syzdek, R. Kostecki, Electrochem. Commun. 13 (2011) 1271–1275.
[14] I. Courtney, J. Dahn, J. Electrochem. Soc. 144 (1997) 2943–2948.
[15] I. Courtney, W. McKinnon, J. Dahn, J. Electrochem. Soc. 146 (1999) 59–68.
[16] B. Scrosati, J. Hassoun, Y. Sun, Energy Environ. Sci. 4 (2011) 3287–3295.
[17] J. Chouvin, C. Branci, J. Sarradin, J. Olivier-Fourcade, J. Jumas, B. Simon, P. Biensan, J. Power Sources 81–82 (1999) 277–281.
[18] J. Chouvin, J. Olivier-Fourcarde, J. Jumas, B. Simon, P. Biensan, J. Electroanal. Chem. 494 (2000) 136–146.
[19] S. Machill, T. Shodai, Y. Sakurai, J.-I. Yamaki, J. Power Sources 73 (1998) 216–223.
[20] J. Xie, N. Imanishi, A. Hirano, Y. Takeda, O. Yamamoto, X. Zhao, G. Cao, Solid State Ionics 181 (2010) 1611–1615.
[21] H. Li, X. Huang, L. Chen, J. Power Sources 81–82 (1999) 340–345.
[22] J. Lee, Y. Xiao, Z. Liu, Solid State Ionics 133 (2000) 25–35.
[23] C.-M. Park, J.-H. Kim, H. Kim, H.-J. Sohn, Chem. Soc. Rev. 39 (2010) 3115–3141.
[24] J. Cabana, L. Monconduit, D. Larcher, M. Palacin, Adv. Mater. 22 (2010) E170–E192.
[25] B. Philippe, A. Mahmoud, J.-B. Ledeuil, M. Sougrati, K. Edström, R. Dedryvere, D. Gonbeau, P.-E. Lippens, Electrochim. Acta 123 (2014) 72–83.
[26] L. Bazin, S. Mitra, P. Taberna, P. Poizot, M. Gressier, M. Menu, A. Barnabe, P. Simon, J.-M. Tarascon, J. Power Sources 188 (2009) 578–582.
[27] G. Elia, S. Panero, A. Savoini, B. Scrosati, J. Hassoun, Electrochim. Acta 90 (2013) 690–694.
[28] H. Bryngelsson, J. Eskhult, L. Nyholm, M. Herranen, O. Alm, K. Edström, Chem. Mater. 19 (2007) 1170–1180.
[29] H. Bryngelsson, J. Eskhult, K. Edström, L. Nyholm, Electrochim. Acta 53 (2007) 102–1073.
[30] J. Torrent-Burgues, E. Guaus, Portugaliae Electrochimica Acta 19 (2001) 247–261.
[31] C. Han, Q. Liu, D. Ivey, Electrochim. Acta 53 (2008) 8332–8340.
[32] A. He, Q. Liu, D. Ivey, J. Mater. Sci. 19 (2008) 553–562.
[33] K. Ui, S. Kikuchi, Y. Kadoma, N. Kumagai, S. Ito, J. Power Sources 189 (2009) 224–229.
[34] A. He, Q. Liu, D. Ivey, J. Mater. Sci.: Mater. Electron. 19 (2008) 553–562.
[35] G. Taillades, N. Benjelloun, J. Sarradin, M. Ribes, Solid State Ionics 152–153 (2002) 119–124.
[36] T. Kulova, A. Skundin, V. Kozhevin, D. Yavsin, S. Gurevich, Russ. J. Electrochem. 46 (2010) 877–881.
[37] A. Pelton, Bulletin of Alloy Phase Diagams 7 (1986) 228–231.
[38] S. Chang, I. Leu, C. Liao, J. Yen, M. Hon, J. Mater. Chem. 14 (2004) 1821–1826.
[39] P. Deacon, M. Mahon, K. Molloy, P. Waterfield, J. Chem. Soc., Dalton Trans. 20 (1997) 3705–3712.
[40] J. Eskhult, M. Herranen, L. Nyholm, J. Electroanal. Chem. 594 (2006) 35–49.
[41] J. Wu, F. Risalvato, S. Ma, X.-D. Zhou, J. Mater. Chem. A 2 (2014) 1647–1651.
[42] S. Cho, J. Yu, K. Kang, D.-Y. Shih, J. Electron. Mater. 34 (2005) 635–642.
[43] Tatge Swanson, Natl. Bur. Stand. (U.S.), Circ. I (1953) 33.
[44] Fuyat Swanson, Natl. Bur. Stand. (U.S.), Circ. II (1953) 12.
[45] H. Okamoto, T. Massalski, Bulletin of Alloy Phase Diagams 5 (1984) 492–503.
[46] J. Moulder, W. Stickle, P. Sobol, K. Bomben, Handbook of X-ray Photoelectron Spectroscopy, Physical Electronics, Inc. (1995).
[47] L. Beaulieu, S. Beattie, T. Hatchard, J. Dahn, J. Electrochem. Soc. 150 (2003) A419–A424.
[48] S. Beattie, T. Hatchard, A. Bonakdarpour, K. Hewitt, J. Dahn, J. Electrochem. Soc. 150 (2003) A701–A705.
[49] K. Shimada, T. Kawaguchi, T. Ichitsubo, E. Matsubara, K. Fukuda, Y. Uchimoto, Z. Ogumi, ECS Transactions 50 (2012) 31–37.
[50] L. Zhao, X. Lai, Q. Niu, C. Li, Advanced Materials Research 512–515 (2012) 1869–1872.
[51] P. Redmond, A. Hallock, L. Brus, Nano Lett. 5 (2005) 131–135.
[52] R. Masitas, F. Zamborini, J. Am. Chem. Soc. 134 (2012) 5014–5017.
[53] M. Valvo, D. Rehnlund, U. Lafont, M. Hahlin, K. Edström, L. Nyholm, J. Mater. Chem. 2 (2014) 9574–9586.
[54] A. Kuhn, F. Argoul, Fractals-Complex Geometry Patterns and Scaling in Nature and Society 1 (1993) 451–459.
[55] G. Trejo, A. Gil, I. Gonzalez, J. Appl. Electrochem. 26 (1996) 1287–1294.
[56] B. Philippe, R. Dedryvere, M. Gorgoi, H. Rensmo, D. Gonbeau, K. Edström, Chem. Mater 25 (2013) 394–404.
[57] B. Philippe, R. Dedryvere, J. Allouche, F. Lindgren, M. Gorgoi, H. Rensmo, D. Gonbeau, K. Edström, Chem. Mater. 24 (2012) 1107–1115.
[58] S. Laruelle, S. Pilard, P. Guenot, S. Grugeon, J.-M. Tarascon, Journal of the Electrochemical Society 151 (2004) A1202–A1209.
[59] G. Aylward, T. Findlay, SI Chemical Data, Wiley, 2008.
[60] C. Housecroft, A. Sharpe, Inorganic Chemistry, Prentice Hall, 2004.
[61] J. Högström, W. Fredriksson, K. Edström, F. Björefors, L. Nyholm, C.-O.A. Olsson, Appl. Surf. Sci. 284 (2013) 700–714.
[62] S. Bouazza, A. Saberi, M. Willert-Porada, Mater. Lett. 65 (2011) 1334–1336.
[63] P. Connor, F. Belliard, M. Behm, L. Tovar, J. Irvine, Ionics 8 (2002) 172–176.
[64] F. Wang, H.-C. Yu, A.V. der Ven, K. Thornton, N. Pereira, Y. Zhu, G. Amatucci, J. Graetz, ECS Transactions 50 (2012) 19–25.
[65] S. Malmgren, K. Ciosek, R. Lindblad, S. Plogmaker, J. Kühn, H. Rensmo, K. Edström, M. Hahlin, Electrochim. Acta 105 (2013) 83–91.
[66] K.C. Högström, S. Malmgren, M. Hahlin, M. Gorgoi, L. Nyholm, H. Rensmo, K. Edström, Electrochim. Acta 138 (2014) 430–436.
[67] S. Malmgren, K. Ciosek, M. Hahlin, T. Gustafsson, M. Gorgoi, H. Rensmo, K. Edström, Electrochim. Acta 97 (2013) 23–32.
[68] M. Fondell, M. Gorgoi, M. Boman, A. Lindblad, J. Electron Spectrosc. Relat. Phenom. 195 (2014) 195–199.
[69] W. Fredriksson, K. Edström, Electrochim. Acta 79 (2012) 82–94.
[70] D. Deng, J. Lee, Chem. Mater. 20 (2008) 1841–1846.
[71] X. Sun, J. Liu, Y. Li, Chem. Mater. 18 (2006) 3486–3494.
[72] L.G. Tovar, P. Connor, F. Belliard, L. Torres-Martinez, J. Irvine, J. Power Sources 97–98 (2001) 258–261.
[73] S. Bouazza, A. Saberi, M. Willert-Porada, Ceram. Int. 38 (2012) 5089–5093.